International Journal for Computational Civil and Structural Engineering, 22(3) 155–174 (2026)

DOI:10.22337/2587-9618-2026-22-3-155-174

LATERAL-TORSIONAL BUCKLING ANALYSIS OF ASYMMETRIC THIN-WALLED BEAMS

Olga A. Tusnina

National Research Moscow State University of Civil Engineering, Moscow, RUSSIA

Abstract: A review and analysis of domestic and international design codes (Eurocode EN 1993-1-1, American standard ANSI/AISC 360-22 and Russian standard SP 16.13330.2017) regarding the lateral-torsional buckling of flexural elements indicate that current standards lack a universal solution for evaluating the lateral-torsional buckling stability of beams with arbitrary cross-sections under arbitrary loading conditions. The available literature provides design recommendations for the buckling analysis of symmetric and asymmetric I-beams and channels under a limited number of loading configurations and boundary conditions. Therefore, evaluating the buckling stability of non-standard beams (such as strengthened sections, which often exhibit complex and asymmetric geometries) is significantly hindered by the absence of practical engineering methods.

This paper proposes a method for analyzing the elastic lateral-torsional buckling stability of thin-walled steel beams with asymmetric cross-sections under arbitrary loading scenarios and boundary conditions. The method is developed based on the analytical solution to a system of differential buckling equations in accordance with Vlasov's thin-walled beam theory, considering the elastic stage of material behavior. The proposed method is formulated in compliance with the design approaches adopted in SP 16.13330.2017, making it suitable for integration into the regulatory framework. The primary advantage of this method lies in its versatility. The validity of the method is confirmed by calculation examples and verification finite element modeling performed using the Simcenter FEMAP with Nastran software suite.

Keywords: lateral-torsional buckling (LTB), thin-walled steel beam, Vlasov's beam theory, elastic critical moment, finite element analysis (FEA)

РАСЧЕТ ИЗГИБНО-КРУТИЛЬНОЙ УСТОЙЧИВОСТИ НЕСИММЕТРИЧНЫХ ТОНКОСТЕННЫХ БАЛОК

О.А. Туснина

Национальный исследовательский Московский государственный строительный университет, г. Москва, РОССИЯ

Аннотация: Обзор и анализ отечественных и зарубежных нормативных методик (Eurocode EN 1993-1-1, ANSI/AISC 360-22, СП 16.13330.2017) расчета общей устойчивости изгибаемых элементов показывает, что в настоящее время в стандартах отсутствует универсальное решение для оценки устойчивости балок произвольного сечения при произвольном загружении. В технической литературе представлены рекомендации по расчету устойчивости симметричных и несимметричных двутавров, а также швеллеров лишь для ограниченного числа расчетных схем и условий закрепления. Расчет устойчивости балок нетипового профиля (например, усиленных сечений, зачастую имеющих сложную асимметричную форму) затруднен из-за отсутствия инженерных методик.

В статье предложена методика расчета устойчивости плоской формы изгиба тонкостенных стальных балок несимметричного сечения при произвольных граничных условиях и вариантах загружения. Преимуществом предлагаемого подхода является его универсальность. Методика разработана на основе аналитического решения системы дифференциальных уравнений устойчивости в соответствии с теорией тонкостенных стержней В.З. Власова в упругой стадии работы материала. Методика представлена в форме, соответствующей расчетным подходам СП 16.13330.2017, что позволяет внедрить ее в нормативный документ. Достоверность методики подтверждена расчетными примерами и верификационным конечно-элементным моделированием, выполненным с использованием ПК Simcenter FEMAP with Nastran.

Ключевые слова: устойчивость плоской формы изгиба; тонкостенные стальные балки, теория тонкостенных стержней Власова, упругий критический момент, метод конечных элементов (МКЭ)

1. INTRODUCTION

Steel beams are susceptible to lateral-torsional buckling (LTB). At a certain critical bending moment (M_{cr}), the beam loses stability. It undergoes combined lateral deflection and twisting.

Design standards regulate the lateral-torsional buckling resistance of beams. A review of domestic and international codes shows a common approach. The critical buckling moment under uniform bending is taken as the baseline value [1,2]. Then, design codes apply correction factors to account for effects like moment gradients, load height, boundary conditions and restraints at the ends of the unbraced length (L_b) of the beam. The number of these factors varies across different design codes. The American specifications ANSI/AISC 360-22 utilize a single-component equation that contains a single equivalent uniform moment factor (C_b). The following equation for critical buckling moment provided by White and Jung [3] is proposed in AISC 360-22 for monosymmetric I-beam:

$$M_{cr} = C_b \frac{\pi^2 E I_y}{L_b^2}\left(\frac{\beta_y}{2} + \sqrt{\left(\frac{\beta_y}{2}\right)^2 + \frac{I_\omega}{I_y}\left(1 + 0.039\frac{I_t}{I_\omega}L_b^2\right)}\right) \tag{1}$$

The single-component AISC equation accounts for loads applied at the shear center of the profile. It does not consider the effect of load height along the cross-section. This equation overestimates the buckling resistance when the load is applied to the compression flange and underestimates when the load is applied to the tension flange.

The comments on the AISC specification provide a refined equation for the critical buckling moment according to guide [4]. This formula was originally derived by Clark and Hill [5]:

$$M_{cr} = C_1 \frac{\pi^2 E I_y}{\left(K_y L_b\right)^2}\sqrt{\left(\frac{K_y}{K_w}\right)^2 \frac{I_\omega}{I_y} + \frac{\left(K_y L_b\right)^2 G I_t}{\pi^2 E I_y} + \left(C_2 y + C_3\frac{\beta_y}{2}\right)^2} + \left(C_2 y + C_3\frac{\beta_y}{2}\right) \tag{2}$$

where y is the coordinate of the load application point relative to the shear center. The factors C_1, C_2 and C_3 depend on the moment diagram. The effective-length factors K_y and K_w – are the effective-length factors correspond to the lateral bending and warping restraint at the ends of the unbraced length L_b, respectively.

Equation (2) is the so-called three-factor formula. It has the most general form that corresponds to the solution of the differential buckling equations. The general solution allows accounting for the influence of cross-section monosymmetry (Wagner coefficient β_y), moment gradient, end-restraint conditions, and load height effects.

The three-factor formula was provided in previous versions of European standard ENV 1993-1-1:1992 [6]. However, the current version of the Eurocode does not contain rules for determining the critical moment. The three-factor formula is used in the NCCI design guidance [7] but, this implementation does not include the coefficient C_3.

The application of the three-factor formula is limited due to the lack of recommendations for determining the factors C_1, C_2 and C_3. For certain specific cases the values of these coefficients are given in guidelines [7, 8].

There are studies on determining these coefficients for specific cases [9-12]. However, these publications mainly focus on simple design models, typical cross-sections of the beams and loading scenarios for simply supported beams. The factor C_3 remains the least studied parameter. This factor accounts for the cross-sectional asymmetry, as well as the offset between the

shear center and the center of gravity. Research on this coefficient is limited, and it is frequently ignored in engineering practice [13].

Therefore, the development of a universal procedure for determining the coefficients C_1, C_2 and C_3 in the three-factor formula is required. This method should accommodate arbitrary loading scenarios, cross-sectional types and boundary conditions.

The Russian code SP 16.13330.2017 specifies lateral-torsional buckling analysis for symmetric and asymmetric I-beams, and channels. The design procedure covers common beam configurations, boundary conditions, and loading scenarios. It also accounts for the load application point along the cross-section height.

However, the SP formulas apply only to specific design cases. These cases are limited to standard structural models and simple loading conditions. Applying the SP methodology to cases not explicitly covered by the code is difficult. The procedure relies on numerous separate formulas and empirical coefficients. This complexity obscures the physical meaning of the design procedure.

An article [14] introduces a refinement to the standard analysis method implemented in the Russian code SP 16.13330.2017. The author proposes a universal formula for the lateral-torsional buckling reduction factor. However, this formula applies only to single-span symmetric I-beams. Furthermore, it is limited to a specific range of loading scenarios.

An effective approach for practical stability analysis is proposed in paper [15]. The author emphasizes the need to develop a unified equation for the lateral-torsional buckling reduction factor. However, the proposed analytical formulas have explicit structural constraints. Their applicability is limited to specific beam geometries and loading conditions.

A solution for the deformation-based buckling analysis of steel members is proposed in [16]. The analysis utilizes a three-dimensional deformed configuration, taking into account material nonlinearity.

The performed review of articles, design codes, and guidelines shows certain limitations. Current literature lacks a unified and exact solution for the lateral-torsional buckling (LTB) analysis of thin-walled members. Specifically, no existing methods cover arbitrary asymmetric cross-sections under arbitrary boundary and loading conditions. Developing such a method is a necessary task.

2. THEORETIICAL STUDY

Consider an arbitrary asymmetric thin-walled profile subjected to a transverse load q_y (Fig. 1). For practical purposes, it is convenient to use a coordinate system with axes parallel to the webs and flanges of the section (the so-called orthogonal X and Y axes with coordinates x and y). The origin is located at the cross-section centroid. The positive Y-axis points toward the tension fibers and the direction of the X-axis is determined by the left-hand rule. The principal coordinate system (X_0, and Y_0 axes with coordinates x_0 and y_0) is inclined at an angle α_0 relative to the orthogonal axes.

The external load q_y acts through the shear center along the Y-axis, parallel to the web.

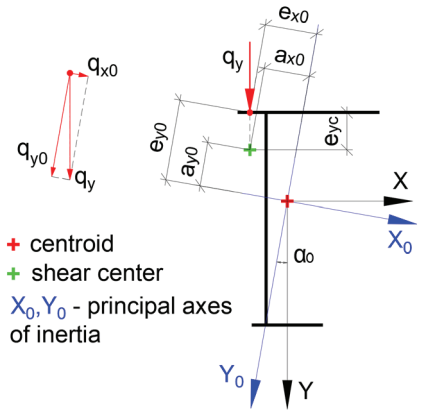


Figure 1. Asymmetric thin-walled profile. Cross-section scheme

Figure 1 defines the geometric and loading parameters of the cross-section: α_0 is the inclination angle of the principal Y_0-axis to the Y-axis; a_{x0} and a_{y0} are the shear center coordinates in

the principal axes of inertia; e_{x0} and e_{y0} are the coordinates of the load application point in the principal axes of inertia; q_{x0} and q_{y0} are the load components parallel to the principal axes, defined as: $q_{xo} = q_y \sin\alpha_0$, $q_{yo} = q_y \cos\alpha_0$.

The transverse load q_y is assumed to act through the shear center thereby eliminating pre-buckling torsion. Thin-walled members with open profiles cross-sections exhibit low torsional stiffness. When a beam is subjected to eccentric transverse loads, its twist angle exceeds he serviceability limit state before reaching the critical buckling load; thus, the serviceability limit state criteria become decisive [17, 18].

For the case under consideration the system of governing linear differential equations for elastic lateral-torsional buckling based on Vlasov's thin-walled beams theory [19] is formulated as follows:

$$\begin{cases} EI_{yo}\xi^{IV} + \left(M_{x0}\theta\right)'' = 0 \\ EI_{yo}\eta^{IV} + \left(M_{y0}\theta\right)'' = 0 \\ EI_{\omega}\theta^{IV} + \left(\left(2\beta_x M_{y0} - 2\beta_y M_{x0} - GI_t\right)\theta'\right)' + \\ + \left(q_{x0}e_{xc0} + q_{y0}e_{yc0}\right)\theta + M_{x0}\xi'' + M_{y0}\eta'' = 0 \end{cases} \quad (3)$$

where I_{x0}, I_{y0} are the principal moments of inertia; I_ω is the warping constant; I_t is the St. Venant torsional constant; β_x, β_y are the monosymmetry constants; $e_{xc0} = e_{x0} - a_{x0}$, $e_{yc0} = e_{y0} - a_{y0}$ are the load application point coordinates relative to the shear center; M_{x0}, M_{y0} are the bending moments about the principal axes: $M_{xo} = M_x \cos\alpha_0$, $M_{yo} = -M_x \sin\alpha_0$.

Equations (3) are formulated with respect to the principal axes of inertia (X_0, Y_0) using the coordinates x_0, y_0. The unknowns in equations (3) are the functions of the shear center displacements: $\xi = \xi(z)$, $\eta = \eta(z)$ are the linear displacements along the X_0 and Y_0 axes, respectively and $\theta = \theta(z)$ is the twist angle about longitudinal axis Z.

The monosymmetry constants βx and βy account for the eccentricity of the centroid relative to the shear center and the additional torque induced by normal bending stresses from the moments M_{y0} and M_{x0} and are defined as follows:

$$\beta_x = \frac{U_{y0}}{2I_{y0}} - a_{x0}, \quad \beta_y = \frac{U_{x0}}{2I_{x0}} - a_{y0} \quad (4)$$

where U_{x0}, U_{y0} are the cross-sectional properties representing the third-order moments of inertia, calculated with respect to the principal axes of inertia:

$$\begin{aligned} U_{x0} &= \int_F y_0^3 dF + \int_F x_0^2 y_0 dF \\ U_{y0} &= \int_F x_0^3 dF + \int_F y_0^2 x_0 dF \end{aligned} \quad (5)$$

The solution to the system of differential buckling equations (3) is described below. From the first and second equations of system (3), the following expressions can be obtained

$$\begin{aligned} \xi'' &= \frac{-M_{x0}}{EI_{y0}} l^2 \cdot \theta = \frac{-M_x \cos\alpha_0}{EI_{y0}} l^2 \cdot \theta \\ \eta'' &= \frac{-M_{y0}}{EI_{x0}} l^2 \cdot \theta = \frac{M_x \sin\alpha_0}{EI_{x0}} l^2 \cdot \theta \end{aligned} \quad (6)$$

By substituting and transforming the system of equations (3), the following buckling equation is obtained:

$$\begin{aligned} &EI_{\omega}\theta^{IV} - 2\beta_{res}\left(M_x\theta'\right)' - GI_t\theta'' + \\ &+ \left(e_{yc} \cdot M_x'' - \frac{M_x^2}{EI_{y0}} l^2 \cdot k_\alpha\right)\theta = 0 \end{aligned} \quad (7)$$

where $k_\alpha = \cos^2\alpha_0 + \frac{EI_{y0}}{EI_{x0}}\sin^2\alpha_0$;

$\beta_{res} = \beta_y \cos\alpha_0 + \beta_x \sin\alpha_0$

Equation (7) can be written in terms of the relative longitudinal coordinate $\zeta = \frac{z}{l}$ (where l is the

unbraced length of the member and z is the absolute longitudinal coordinate).
The following definitions can be defined:

$$\kappa(\zeta)=\frac{l}{EI_{y0}}\cdot M_x(\zeta)$$
$$a=\frac{EI_\omega}{l^2GI_t},\ b_1=\frac{2\beta_{res}EI_{y0}}{lGI_t},\ b_2=\frac{e_{yc}EI_{y0}}{lGI_t}, \quad (8)$$
$$c=\frac{EI_{y0}}{GI_t}k_\alpha$$

Then, the buckling equation (7) is expressed as follows:

$$a\theta^{IV}-\theta''-b_1(\kappa\theta')'+\left(b_2\kappa''-c\kappa^2\right)\theta=0 \quad (9)$$

The components of equation (9) account for the factors affecting lateral-torsional buckling:
- parameter b_1 reflects the effect of cross-sectional asymmetry and the eccentricity between the center of gravity and the shear center;
- parameter b_2 accounts for the load application point along the cross-section height, representing either the destabilizing or restoring effect of the load.
The function $\kappa(\zeta)$ in equation (9) describes the bending moments distribution $M_x(\zeta)$ along the unbraced length of the beam (bending moment diagram). The moment distribution is a function of the external load: $M_x(\zeta)=f(q_y)$. Thus, solving equation (9) yields the critical load value $q_{y,cr}$ at which lateral-torsional buckling occurs.
To solve the equation (9), a sinusoidal distribution of the twist angles is assumed along the unbraced length: $\theta=A\sin\pi\zeta$ $(\zeta\in[0;1])$. Applying the Bubnov–Galerkin method, the differential equation of stability is expressed as follows:

$$\int_0^1\left(\left(b_1+4b_2\right)\kappa+\frac{c}{\pi^2}\kappa^2\right)\cos2\pi\zeta\,d\zeta+$$
$$+\int_0^1\left(b_1\kappa-\frac{c}{\pi^2}\kappa^2\right)d\zeta+\left(a\pi^2+1\right)=0 \quad (10)$$

Equation (10) can be transformed as follows:

$$b_1\left(\int_0^1\kappa\cos2\pi\zeta\,d\zeta+\int_0^1\kappa d\zeta\right)+4b_2\int_0^1\kappa\cos2\pi\zeta\,d\zeta+$$
$$+\frac{c}{\pi^2}\left(\int_0^1\kappa^2\cos2\pi\zeta\,d\zeta-\int_0^1\kappa^2d\zeta\right)+\left(a\pi^2+1\right)=0 \quad (11)$$

The following definitions are introduced:

$$\int_0^1\kappa\cos2\pi\zeta\,d\zeta=\lambda\cdot A_B$$
$$\int_0^1\kappa\cos2\pi\zeta\,d\zeta+\int_0^1\kappa d\zeta=\lambda\cdot C_B \quad (12)$$
$$\int_0^1\kappa^2\cos2\pi\zeta\,d\zeta-\int_0^1\kappa^2d\zeta=\lambda^2\cdot D_B$$

where parameter $\lambda=\frac{l}{EI_{y0}}\cdot q_yl^2$

Thus, equation (11) becomes:

$$\left(b_1\cdot C_B+4A_B\cdot b_2\right)\lambda-\frac{c}{\pi^2}D_B\lambda^2+\left(a\pi^2+1\right)=0 \quad (13)$$

The dimensionless parameters in Equations (12) are given by:

$$A_B=\frac{\int_0^1M_x(\zeta)\cos2\pi\zeta\,d\zeta}{q_yl^2}$$
$$C_B=\frac{\int_0^1M_x(\zeta)\cos2\pi\zeta\,d\zeta+\int_0^1M_x(\zeta)d\zeta}{q_yl^2} \quad (14)$$
$$D_B=\frac{\int_0^1M_x^2(\zeta)d\zeta-\int_0^1M_x^2(\zeta)\cos2\pi\zeta\,d\zeta}{\left(q_yl^2\right)^2}$$

Introducing the parameter $\rho=-4\pi^2A_B$, the final form of the buckling equation can be written as follows:

$$\frac{c}{\pi^2}\lambda^2 - \left(b_1 \cdot \frac{C_B}{D_B} + \frac{1}{D_B} \cdot \rho \cdot \frac{b_2}{\pi^2}\right) \cdot \lambda - \\ - \frac{1}{D_B}\left(a\pi^2 + 1\right) = 0 \tag{15}$$

By solving the quadratic equation (15), the value of λ_{cr} at which the beam buckling occurs is determined:

$$\lambda_{cr} = \left(\frac{\pi^2}{2c} \cdot \left(b_1 \frac{C_B}{D_B} + \frac{1}{D_B}\rho\frac{b_2}{\pi^2}\right) + \right. \\ \left. + \sqrt{\frac{\pi^4}{4c^2} \cdot \left(b_1 \frac{C_B}{D_B} + \frac{1}{D_B}\rho\frac{b_2}{\pi^2}\right)^2 + \frac{1}{D_B}\frac{\pi^2\left(1+\pi^2 a\right)}{c}}\right. \tag{16}$$

Then, the critical load $q_{y,cr}$ and the critical moment M_{cr} can be expressed as follows:

$$M_{cr} = K_1 \cdot q_{y,cr} l^2 = K_1 \cdot \frac{EI_{y0}}{l} \cdot \lambda_{cr} \tag{17}$$

The coefficient K_1 in formula (17) is determined by the bending moment diagram and the specific cross-section along the beam length where the moment value is calculated.

Substituting the values of the parameters a, b_1, b_2, c from (8) into formula (16), we introduce the following coefficients:

$$C_I = \frac{K_I}{\sqrt{D_B}}, C_{II} = \frac{\rho}{\sqrt{D_B}}, C_{III} = \frac{C_B}{\sqrt{D_B}} \tag{18}$$

In its final form, the equation for the elastic lateral-torsional buckling critical moment is expressed as follows:

$$M_{cr} = C_I \left(\frac{\pi^2 EI_{y0}}{k_\alpha l^2}\left(C_{III} \cdot \beta_{res} + \frac{e_{y,c}}{2\pi^2} \cdot C_{II}\right) + \sqrt{\frac{\pi^2 EI_{y0}}{k_\alpha l^2}\left(\frac{\pi^2 EI_{y0}}{k_\alpha l^2}\left(C_{III} \cdot \beta_{res} + \frac{e_{y,c}}{2\pi^2} \cdot C_{II}\right)^2 + \frac{\pi^2 EI_\omega}{l^2} + GI_t\right)}\right) \tag{19}$$

In fact, the derived formula (19) represents an analogue of the three-factor equation for the critical moment (see equation (2)). The key difference is that formula (19) is written in a generalized form and can be applied to any cross-sectional shape, which is highly relevant, for instance, when analyzing strengthened structures. Furthermore, formula (19) enables the analysis of lateral-torsional buckling under unsymmetrical bending, i.e., when the load does not act within a principal plane of inertia.

In the general case, calculating with formula (19) requires knowing the cross-sectional geometric properties, the coordinates of the shear center and the centroid, the inclination angle of the principal axes of inertia, and the load application point coordinates, as well as computing the coefficients C_I, C_{II} и C_{III}.

When applying formula (19) in practice, certain difficulties may arise. These primarily concern the determination of the warping constant I_ω and the parameter β_{res}. Its components β_x and β_y incorporate the geometric properties U_{x0} and U_{y0}, which represent third-order moments of inertia and require the evaluation of integrals over the cross-sectional area. However, existing methods of structural mechanics enable these computations for any cross-sectional shape. For common section types (e.g., asymmetric I-beams and channels), simplified formulas [20] and tabular solutions can be recommended. Standard rolled section catalogs can be supplemented with the respective values.

Furthermore, an automated computational tool for evaluating the geometric properties of arbitrary thin-walled cross-sections will be developed within the framework of future research.

The primary difficulty in applying formula (19) lies in determining the coefficients C_I, C_{II} and C_{III}. These coefficients incorporate the integral parameters A_B, C_B and D_B, that account for both the shape of the bending moment diagram and the buckling mode.

To evaluate the parameters A_B, C_B and D_B, the moment distribution function $M_x(\zeta)$ along the member length must be defined for integration

according to (12). In practice, analytical calculations are hindered by the complexity of deriving moment functions and the labor-intensiveness of manual integration (16). Actual bending moment diagrams are rarely described by simple functions. Therefore, design codes must not be limited only to special loading cases. A universal engineering method for lateral-torsional buckling analysis is required. This methodology must account for arbitrary moment diagrams, any boundary conditions, and diverse buckling modes.

3. ANALYTICAL SOLUTION

The coefficients C_I, C_{II} and C_{III} were analytically determined for various bending moment diagram cases. For this purpose, the actual bending moment diagram within the unbraced segment is approximated by the function $M_x(\zeta)$. Next, by defining the buckling mode shape as a function of the twist angle distribution $\theta = A\sin\pi\zeta$, the integral parameters for the differential equations were evaluated

The most characteristic beam buckling modes were identified using finite element analysis (FEA). As a rule, the lateral-torsional buckling of a beam occurs within the span. This phenomenon involves out-of-plane displacement and twisting toward the compressed top flange. This buckling mode is defined as the "mid-span" buckling mode.

Under specific loading configurations, continuous beams with a less developed bottom flange exhibited a distinct buckling mode. This mode involves out-of-plane displacement of the compressed bottom flange near the support (Fig. 2). This phenomenon is defined as the "support-zone" buckling mode. Here, buckling occurs along the compressed bottom flange within the beam segments on the left and right sides of support.

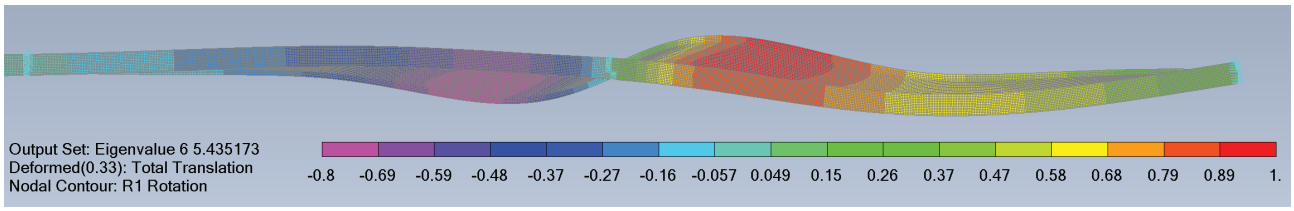
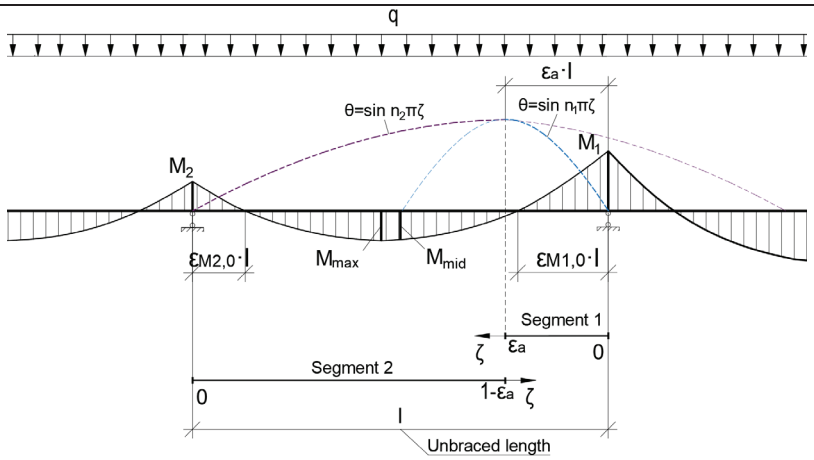


Figure 2. Support-zone buckling mode: lateral-torsional buckling in the bottom-flange compression zones near the support

Table 1. Design models adopted to determine the coefficients C_I, C_{II} and C_{III} for the mid-span buckling mode

Bending moment diagram	Design model and equations for approximating the bending moment diagram
1.1 Non-linear moment diagram	

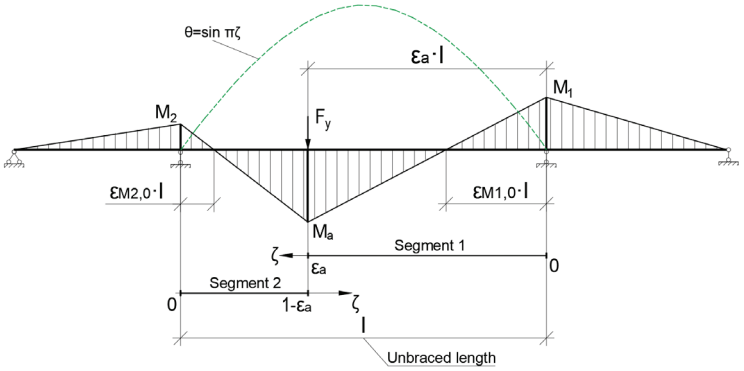
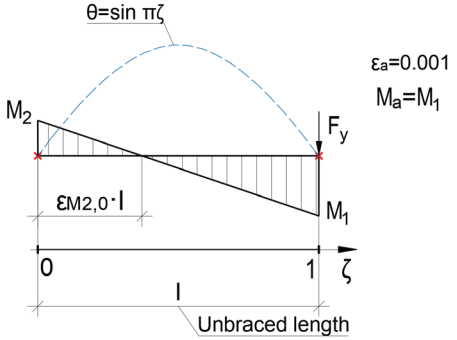
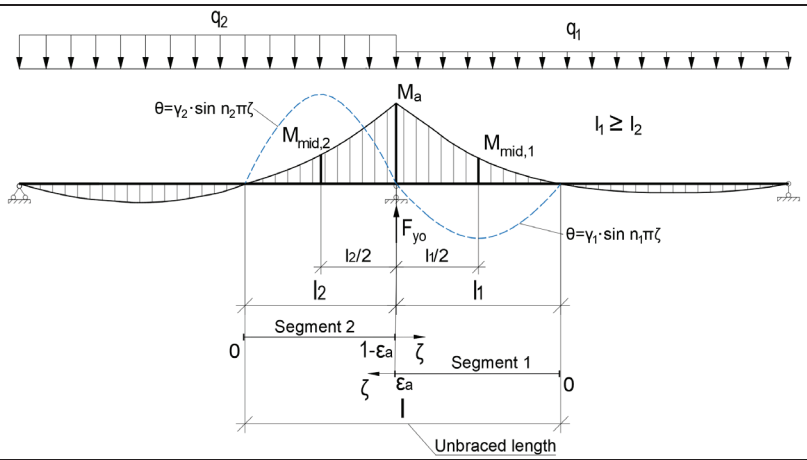
	$$M_x(\zeta)=\begin{cases} q_y l^2\cdot\left(a_{M1}\zeta^2+b_{M1}\zeta+c_{M1}\right),\zeta\in[0;\varepsilon_a](segment\ 1) \\ q_y l^2\cdot\left(a_{M2}\zeta^2+b_{M2}\zeta+c_{M2}\right),\zeta\in[0;(1-\varepsilon_a)](segment\ 2)\end{cases}$$
2.2 Piecewise linear moment diagram with a single kink	 $$M_x(\zeta)=\begin{cases} F_y l\cdot\left(b_{F1}\zeta+c_{F1}\right),\zeta\in[0;\varepsilon_a](segment\ 1) \\ F_y l\cdot\left(b_{F2}\zeta+c_{F2}\right),\zeta\in[0;(1-\varepsilon_a)](segment\ 2)\end{cases}$$
1.3 Linear moment diagram without kinks	 $$M_x(\zeta)=F_y l\cdot\left(b_F\zeta+c_F\right),\zeta\in[0;1]$$

Table 2. Design models adopted to determine the coefficients C_I, C_{II} and C_{III} for the support-zone buckling mode

Bending moment diagram	Design model and equations for approximating the bending moment diagram
2.1 Non-linear moment diagram	

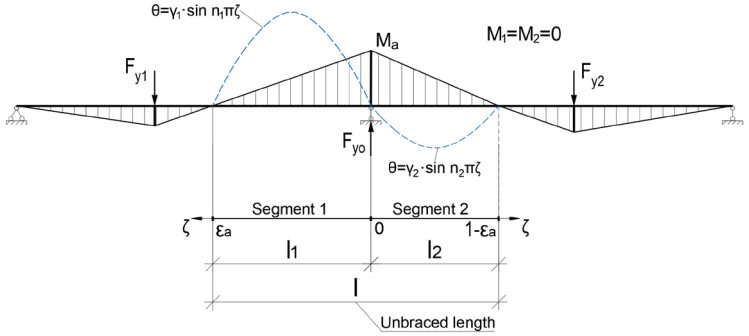
	$$M_x(\zeta)=\begin{cases}F_{yo}l\cdot\left(l_{M1}\zeta^2+d_{M1}\zeta\right),\zeta\in\left[0;\varepsilon_a\right](segment\ 1)\\ F_{yo}l\cdot\left(l_{M2}\zeta^2+d_{M2}\zeta\right),\zeta\in\left[0;\left(1-\varepsilon_a\right)\right](segment\ 2)\end{cases}$$
2.2 Piecewise linear moment diagram	 $$M_x(\zeta)=\begin{cases}F_{yo}l\cdot\left(d_{F1}\zeta+e_{F1}\right),\zeta\in\left[0;\varepsilon_a\right](segment\ 1)\\ F_{yo}l\cdot\left(d_{F2}\zeta+e_{F2}\right),\zeta\in\left[0;\left(1-\varepsilon_a\right)\right](segment\ 2)\end{cases}$$

Table 1 presents the design models adopted to determine the coefficients *C_I, C_{II} and C_{III}* under various bending moment diagrams along the unbraced length for the mid-span lateral-torsional buckling mode. The design models for the support-zone buckling mode are represented in Table 2.

4. PROPOSED ENGINEERING METHOD

For practical application, analytical formulas and tabular solutions have been developed to determine the coefficients *C_I, C_{II} and C_{III}* under various bending moment distributions. Two types of lateral-torsional buckling modes are defined: mid-span and support-zone.

I. Mid-span buckling mode. The following bending moment diagram configurations are considered:

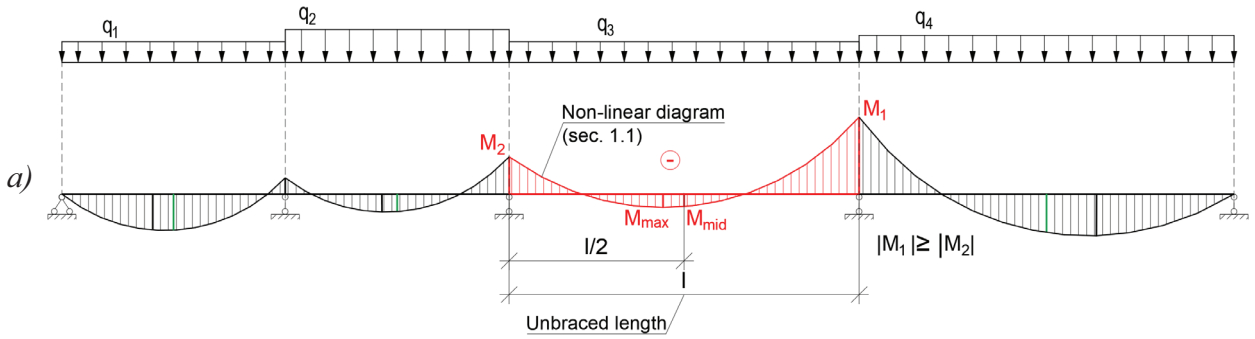
1.1. Non-linear moment diagram.

1.2. Piecewise linear moment diagram with a single kink.

1.3. Linear moment diagram without kinks.

1.4. Piecewise linear moment diagram with two or more kinks.

The design models adopted for the mid-span lateral-torsional buckling check of a continuous beam under various bending moment diagrams are presented in Figure 3.



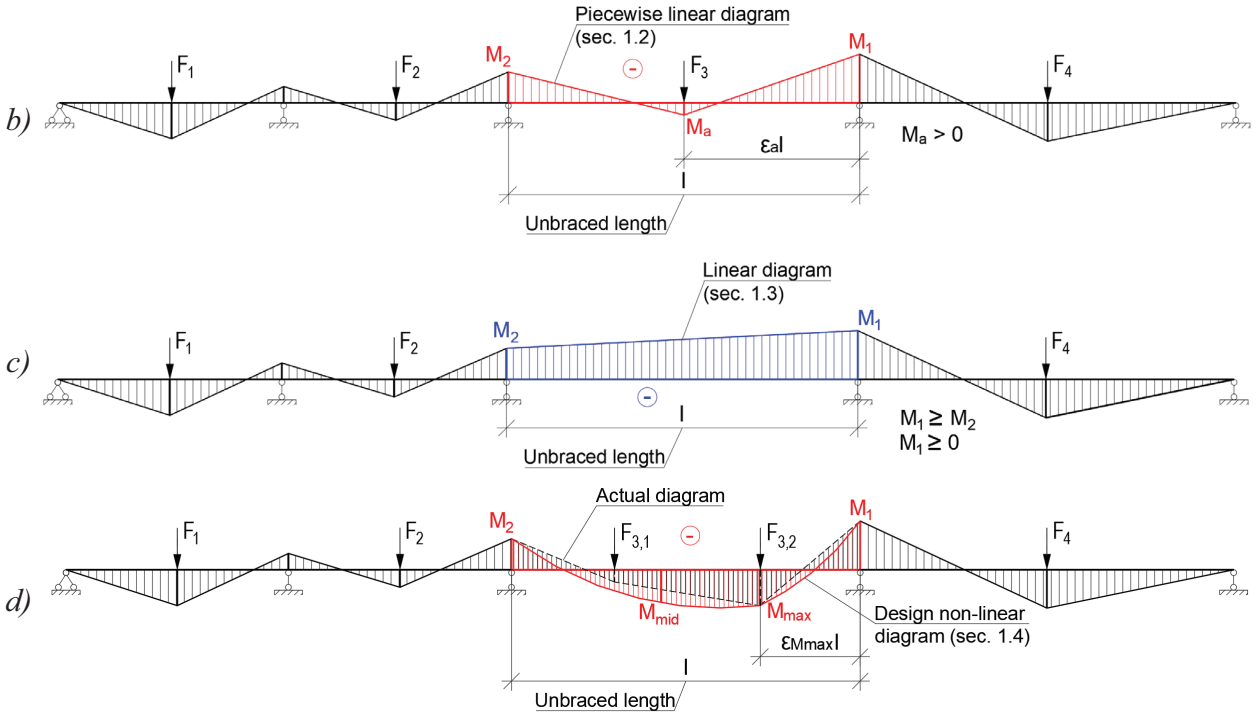


Figure 3. Mid-span buckling mode. Design models for the bending moment diagram: a) non-linear; b) piecewise linear with a single kink; c) linear; d) piecewise linear with two or more kinks

1.1. Non-linear moment diagram (Fig. 3, a).

The coefficients C_I, C_{II} and C_{III} are:

$$C_I = \frac{5.48 \cdot \pi^2 \cdot M_{\max}}{\sqrt{125.5 \cdot \left(M_1^2 + M_2^2\right) + 2278.55 \cdot M_{mid}^2 + 261.81 \cdot \left(M_1 + M_2\right) - 130.91 \cdot M_1 M_2}}$$

$$C_{II} = \frac{21.91 \cdot \pi^2 \cdot \left(2M_{mid} - M_2 - M_1\right)}{\sqrt{125.5 \cdot \left(M_1^2 + M_2^2\right) + 2278.55 \cdot M_{mid}^2 + 261.81 \cdot \left(M_1 + M_2\right) - 130.91 \cdot M_1 M_2}}$$

$$C_{III} = \frac{14.5 \cdot \left(M_1 + M_2\right) + 25.1 \cdot M_{mid}}{\sqrt{125.5 \cdot \left(M_1^2 + M_2^2\right) + 2278.55 \cdot M_{mid}^2 + 261.81 \cdot \left(M_1 + M_2\right) - 130.91 \cdot M_1 M_2}}$$

1.2. Piecewise linear moment diagram with a single kink (Fig. 3, b)

The coefficients C_I, C_{II} and C_{III} are determined using the following formulas:

$$C_I = \frac{K_I}{\sqrt{D_B}}, C_{II} = \frac{\rho}{\sqrt{D_B}}, C_{III} = \frac{C_B}{\sqrt{D_B}}$$

where $K_1 = \dfrac{M_a \cdot \left(1 - \varepsilon_a\right) \cdot \varepsilon_a}{M_a - M_1 \cdot \left(1 - \varepsilon_a\right) - M_2 \cdot \varepsilon_a}$

The parameters D_B, C_B and ρ determined as a function of the relative position of the kink ε_a using the design charts presented in Fig. 4–6.

Parameter D_B is given by: $D_B = D_{B,1} + D_{B,2}$,

$$D_{B,1} = b_{F1}^2 K_{D,bF1} + c_{F1}^2 K_{D,cF1} + b_{F1} c_{F1} K_{D,bF1cF1}$$

$$D_{B,2} = b_{F2}^2 K_{D,bF2} + c_{F2}^2 K_{D,cF2} + b_{F2} c_{F2} K_{D,bF2cF2}$$

Parameter C_B is given by: $C_B = C_{B,1} + C_{B,2}$,

$$C_{B,1} = b_{F1} \cdot K_{C,bF1} + c_{F1} \cdot K_{C,cF1}$$

$$C_{B,2} = b_{F1} \cdot K_{C,bF2} + c_{F1} \cdot K_{C,cF2}$$

The coefficients b_F и c_F characterize the moment distribution and equal:

$$c_{F1} = \frac{M_1 \cdot (1-\varepsilon_a) \cdot \varepsilon_a}{M_a - M_1 \cdot (1-\varepsilon_a) - M_2 \cdot \varepsilon_a};$$

$$b_{F1} = \frac{(M_a - M_1) \cdot (1-\varepsilon_a)}{M_a - M_1 \cdot (1-\varepsilon_a) - M_2 \cdot \varepsilon_a};$$

$$c_{F2} = \frac{M_2 \cdot (1-\varepsilon_a) \cdot \varepsilon_a}{M_a - M_1 \cdot (1-\varepsilon_a) - M_2 \cdot \varepsilon_a};$$

$$b_{F2} = \frac{(M_a - M_2) \cdot \varepsilon_a}{M_a - M_1 \cdot (1-\varepsilon_a) - M_2 \cdot \varepsilon_a};$$

The coefficients K_D и K_C are represented in Fig. 4 and 5. Parameter ρ is given in Table 3 and Fig. 6.

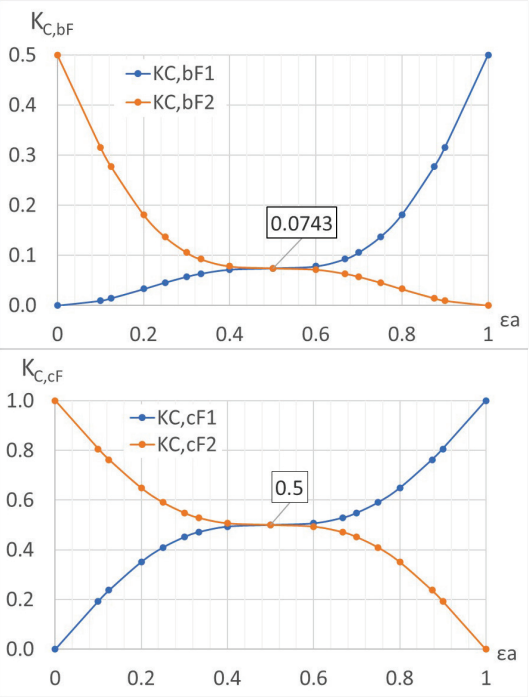


Figure 4. Design charts for the K_C coefficients for a piecewise linear bending moment diagram

Table 3. Parameter ρ for a piecewise linear bending moment diagram with a kink

ε_a	0	0.125	0.25	0.333	0.5	0.667	1
ρ	0	0.293	1	1.5	2	1.5	1

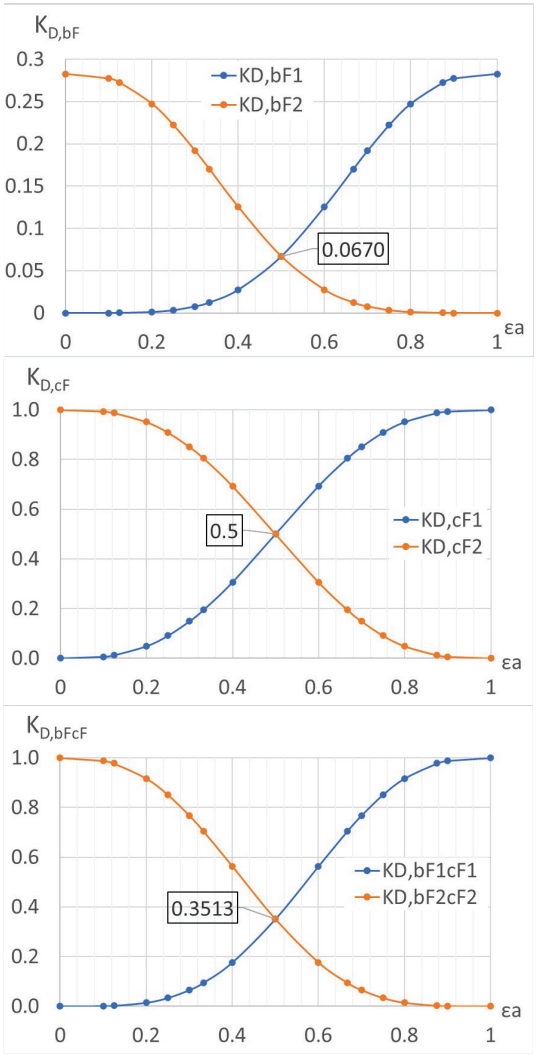


Figure 5. Design charts for the K_D coefficients for a piecewise linear bending moment diagram

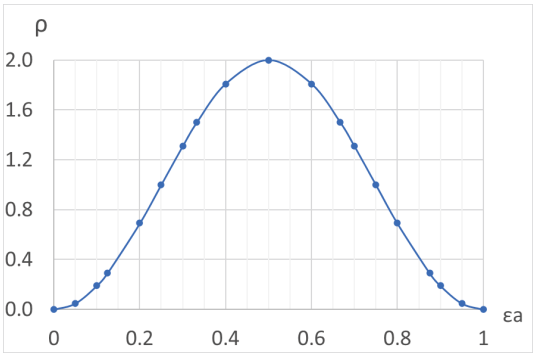
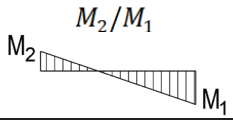


Figure 6. Design chart for the parameter ρ for a piecewise linear bending moment diagram

1.3. Linear moment diagram (Fig. 3, c)

The coefficients C_I, C_{II} and C_{III} are determined as a function of the end-moment ratio M_2 / M_1 and presented in Table 4 and Fig. 7.

Table 4. Coefficients C_I, C_{II} and C_{III} for a linear moment diagram without kinks

M_2/M_1 	C_I	C_{II}	C_{III}
-1	2.765	0	0
-0.5	2.711	0	0.678
-0.25	2.284	0	0.856
0	1.881	0	0.94
0.25	1.564	0	0.977
0.5	1.324	0	0.993
1	1	0	1

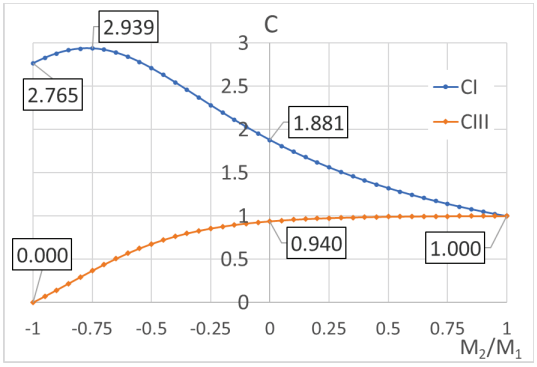


Figure 7. Design charts for the C_I, C_{II} and C_{III} coefficients for a linear moment diagram

1.4. Piecewise linear moment diagram with two or more kinks (Fig. 3, d)

The following initial design data are specified: M_{max} is the maximum moment within the span (at one of the kinks); M_1, M_2 are the support moments (M_1 is the larger of the support moments in absolute value ($|M_1| \geq |M_2|$)).

A piecewise linear bending moment diagram with two or more kinks within the span is reduced to an equivalent non-linear diagram.

For this purpose, the mid-span moment value M_{mid} on the equivalent parabolic bending moment diagram is determined by the formula:

$$M_{mid} = \frac{M_1 \cdot (4\varepsilon_{M\max} - 3) + M_2 \cdot (4\varepsilon_{M\max} - 1)}{8\varepsilon_{M\max} - 1}$$

where ε_{Mmax} is the relative coordinate of the maximum moment (from the end with moment M_1).

The subsequent calculation is performed in accordance with Section 2.1 as for a non-linear bending moment diagram.

II. Support-zone buckling mode

The following bending moment diagram configurations are considered (Fig. 8):

2.1. Non-linear moment diagram.

2.2. Piecewise linear moment diagram.

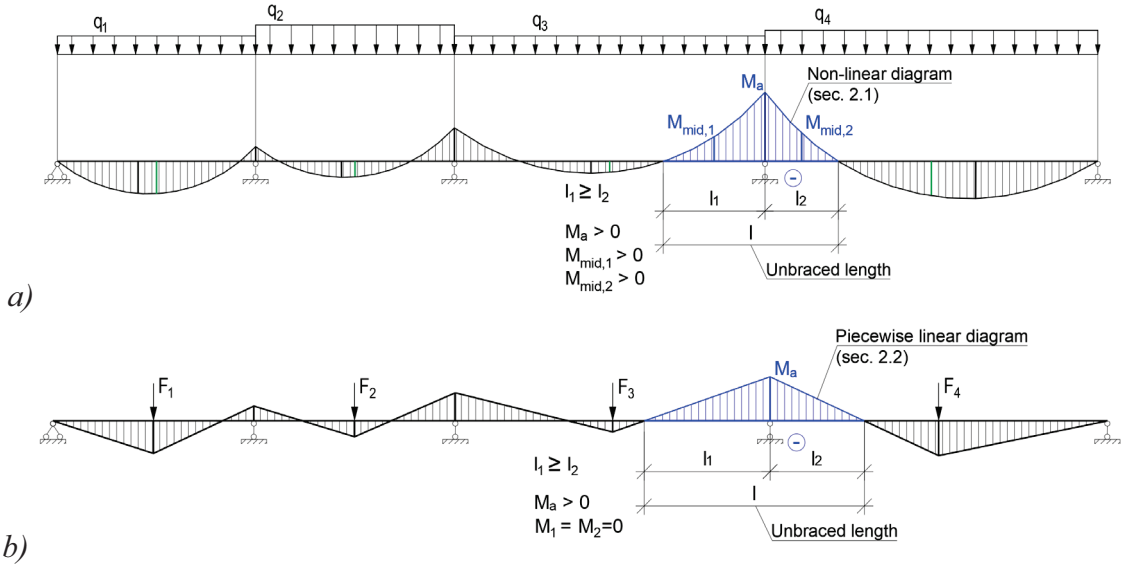


Figure 8. Support-zone buckling mode. Design models for various configurations of the bending moment diagram: a) non-linear; b) piecewise linear with a single kink

2.1. Non-linear moment diagram (Fig. 8, a).
Input data: l_1, l_2 are the lengths of the beam segments with the bottom flange in compression ($l_1 \geq l_2$); M_a is the bending moment at the support; $M_{mid,1}$ and $M_{mid,2}$ are the bending moments at the midpoint of the 1st and 2nd segment correspondingly; $l = l_1 + l_2$ is the equivalent unbraced length; $\varepsilon_a = l_1 / l$ is the relative coordinate.
The coefficients C_I, C_{II} and C_{III} are:

$$C_I = \frac{K_I}{\sqrt{D_B}}, C_{II} = \frac{\rho}{\sqrt{D_B}}, C_{III} = \frac{C_B}{\sqrt{D_B}}$$

where $K_1 = (1-\varepsilon_a)\cdot\varepsilon_a$

$$\rho = \frac{8\cdot(1-\varepsilon_a)\cdot(M_{mid,1} + M_{mid,2} - M_a)}{M_a}$$

Parameter D_B

$$D_B = \left(\frac{\varepsilon_a^4}{5} - \frac{\varepsilon_a^2}{\pi^2} + \frac{3}{2\pi^4}\right)\cdot\frac{4M_{L1}^2}{M_a^2}\cdot\frac{(1-\varepsilon_a)^2}{\varepsilon_a} +$$
$$+\left(\frac{(1-\varepsilon_a)^3\cdot\varepsilon_a}{5} - \frac{(1-\varepsilon_a)^2}{\pi^2} + \frac{3}{2\pi^4}\right)\cdot\frac{4M_{L2}^2}{M_a^2}\cdot\varepsilon_a +$$
$$+\left(\frac{\varepsilon_a^3}{2} - \frac{3\varepsilon_a}{2\pi^2}\right)\cdot\frac{2M_{L1}M_{D1}}{M_a^2}\cdot(1-\varepsilon_a)^2 +$$
$$+\left(\frac{(1-\varepsilon_a)^3\cdot\varepsilon_a}{2} - \frac{3(1-\varepsilon_a)^2}{2\pi^2}\right)\cdot\frac{2M_{L1}M_{D1}}{M_a^2}\cdot\varepsilon_a +$$
$$+\left(\frac{\varepsilon_a^3}{3} - \frac{\varepsilon_a}{2\pi^2}\right)\cdot\frac{M_{D1}^2}{M_a^2}\cdot(1-\varepsilon_a)^2 +$$
$$+\left(\frac{(1-\varepsilon_a)^2\cdot\varepsilon_a}{3} - \frac{(1-\varepsilon_a)}{2\pi^2}\right)\cdot\frac{M_{D2}^2}{M_a^2}\cdot\varepsilon_a\cdot(1-\varepsilon_a)$$

Parameter C_B

$$C_B = \frac{\varepsilon_a\cdot(1-\varepsilon_a)}{2}\cdot\left(\frac{M_{D1}}{M_a}\cdot\varepsilon_a + \frac{M_{D2}}{M_a}\cdot(1-\varepsilon_a)\right) +$$
$$+\left(\frac{\varepsilon_a^2}{3} + \frac{1}{2\pi^2}\right)\cdot\frac{2M_{L1}}{M_a}\cdot(1-\varepsilon_a) +$$
$$+\left(\frac{(1-\varepsilon_a)\cdot\varepsilon_a}{3} + \frac{1}{2\pi^2}\right)\cdot\frac{2M_{L2}}{M_a}\cdot(1-\varepsilon_a)$$

The values of the moments are calculated:

$$M_{D1} = 4M_{mid,1} - M_a,\ M_{D2} = 4M_{mid,2} - M_a;$$
$$M_{L1} = M_a - 2M_{mid,1},\ M_{L2} = M_a - 2M_{mid,2}$$

2.2. Piecewise linear moment diagram (Fig. 8, b). The coefficients C_I, C_{II} and C_{III} are:

$$C_I = \sqrt{\frac{\varepsilon_a}{(0.333\cdot\varepsilon_a - 0.101)}}, C_{II} = 0, C_{III} = 0.5C_I$$

where $\varepsilon_a = l_1 / l$ is the relative coordinate; l_1, l_2 are the lengths of the beam segments adjacent to the support where the bottom flange is in compression (where $l_1 \geq l_2$); $l = l_1 + l_2$ is the equivalent unbraced length.
To identify the governing lateral-torsional buckling mode, the minimum buckling load factor k_{buckl} among those calculated for the different modes must be determined: $k_{buckl} = \frac{M_{cr}}{M_{\max}}$,
where M_{max} is the maximum moment in the span for a mid-span mode and the moment at the support $M_{\max} = M_a$ for a support-zone mode.

5. FINITE ELEMENT VERIFICATION

A lateral-torsional buckling analysis of the continuous beam (Fig. 9) is performed using the developed method. To verify the procedure, a finite element buckling analysis of the beam was performed using the FEMAP software suite. The beam model was built using 4-node shell elements (CQUAD4). The linear elastic buckling analysis was carried out via the Nas-

tran solver using Solution 105 (SOL 105), which determines the critical loads by solving a generalized eigenvalue problem. The SOL 105 solver evaluates the ideal elastic stability (bifurcation buckling). It does not account for the following factors: initial geometric imperfections, residual stresses in the steel due to welding or hot-rolling processes and material non-linearity (plastic deformations and steel yielding).

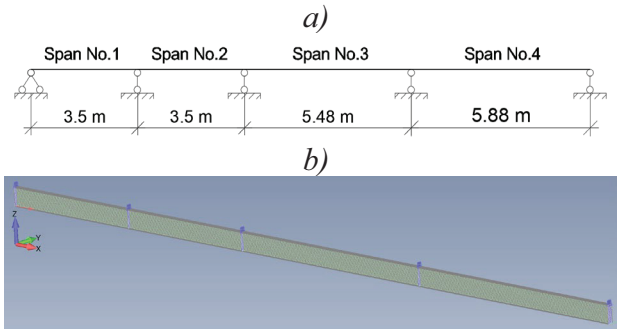


Figure 9. Considered continuous beam a) design model; b) finite element model

Load cases (Fig. 10): 1. L1 – concentrated load F_y=150 kN in each span. 2. L1q – uniformly distributed load q_y=100 kN/m in each span. 3. L2q – uniformly distributed load q_y=100 kN/m in alternative spans (span No. 1 and No. 3).

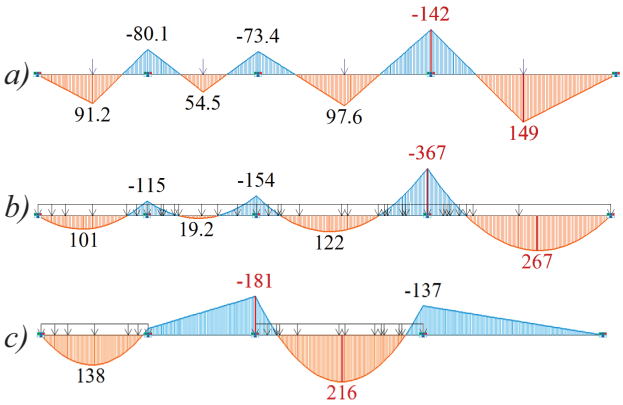


Figure 10. Bending moment diagrams for load case: a) L1; b) L1q; c) L2q

Boundary conditions (Fig. 11). Bottom-flange and top-flange supported beams are considered in the finite element analysis. Various structural configurations of beam supports and bracing are considered, including beams without stiffeners, beams with end bearing stiffeners only, and beams with stiffeners at each support. Double-sided stiffeners with a thickness of 10 mm and a width of 50 mm are modeled.

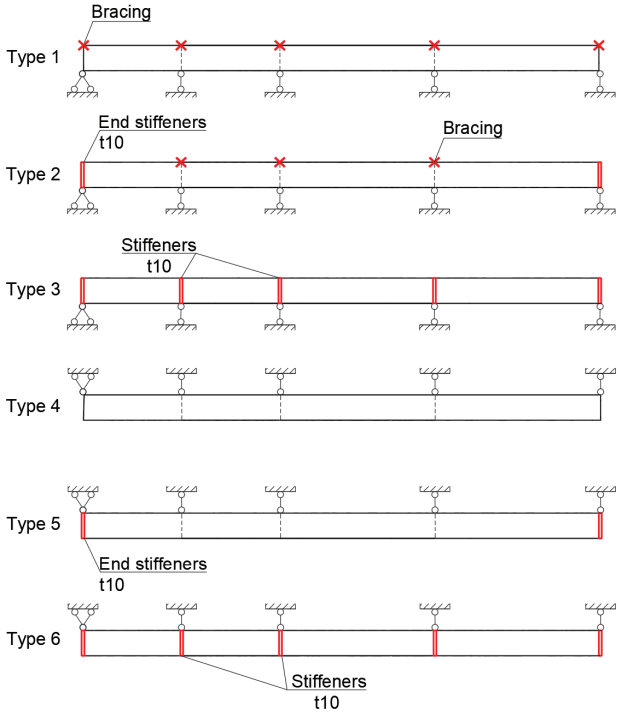


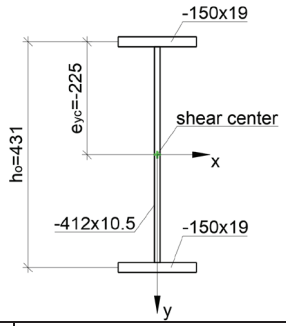
Figure 11. Boundary conditions

For bottom-flange supported beams, lateral bracing at the supports is provided either by stiffeners or by direct lateral restraints applied to the top flange. For beams without bearing stiffeners, the lateral displacement of the top flange at the supports is restricted. No intermediate bracing is provided within the spans.

Tables 5–7 present a comparison of the critical moment values calculated by the proposed method (formula (19)) with the finite element analysis data for the symmetric and monosymmetric I-beams.

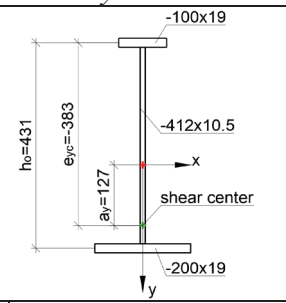
The “FEMAP” column presents the minimum critical moment values obtained from the finite element analysis among all analyzed types of boundary conditions (see Fig. 11).

Table 5. Comparison of Critical Buckling Moments M_{cr}. Symmetric I-beam



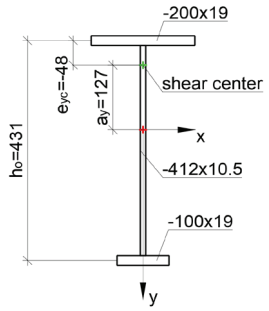
Load case	Span	M_{cr}, kNm (Top flange loaded)		
		Proposed method	FEMAP	Error Δ
L1	No. 1	420	457	8.1%
	No. 2	312	332	6.0%
	No. 3	214	258	17.1%
	No. 4	230	240	4.2%
L1q	No. 1	372	413	9.9%
	No. 2	101	99	-2.0%
	No. 3	151	185	18.4%
	No. 4	199	212	6.1%
L2q	No. 1	407	482	15.6%
	No. 2	852	1048	18.7%
	No. 3	205	226	9.3%
	No. 4	463	614	24.6%
Load case	Span	M_{cr}, kNm (Bottom flange loaded)		
		Proposed method	FEMAP	Error Δ
L1	No. 4	603	635	5.0%
L1q	No. 4	478	496	3.6%
L2q	No. 3	533	652	18.3%
	No. 4	463	617	25.0%

Table 6. Comparison of Critical Buckling Moments M_{cr}. Monosymmetric I-section (type 1)



Load case	Span	M_{cr}, kNm (Top flange loaded)		
		Proposed method	FEMAP	Error Δ
L1	No. 1	227	206	-10.2%
	No. 2	197	196	-0.5%
	No. 3	152	143	-6.3%
	No. 4	156	137	-13.9%
L1q	No. 1	195	191	-2.1%
	No. 2	74	72	-2.8%
	No. 3	106	115	7.8%
	No. 4	133	127	-4.7%
L2q	No. 1	206	225	8.4%
	No. 3	130	126	-3.2%
	No. 4	777	806	3.6%
Load case	Span	M_{cr}, kNm (Bottom flange loaded)		
		Proposed method	FEMAP	Error Δ
L1	No. 4	470	396	-18.7%
L1q	No.1	662	759	12.8%
	No.4	359	300	-19.7%
L2q	No. 1	474	503	5.8%
	No. 3	384	389	1.3%
	No. 4	777	966	19.6%

Table 7. Comparison of Critical Buckling Moments M_{cr}. Monosymmetric I-section (type 2)



Load case	Span	M_{cr}, kNm (Top flange loaded)		
		Proposed method	FEMAP	Error Δ
L1	No. 2	314	325	3.4%
	No. 3	262	312	16.0%
	No. 4	337	330	-2.1%
L1q	No. 1	601	608	1.2%
	No. 2	80	85	5.9%
	No. 3	185	208	11.1%
	No. 4	302	292	-3.4%
L2q	No. 1	729	707	-3.1%
	No. 2	441	569	22.5%
	No. 3	318	363	12.4%
	No. 4	315	372	15.3%
Load case	Span	M_{cr}, kNm (Bottom flange loaded)		
		Proposed method	FEMAP	Error Δ
L1	No. 4	667*	737	9.5%
L1q	No. 4	1027*	1066	3.7%
L2q	No. 2	441	584	24.5%
	No. 4	315	375	0.16

* support-zone buckling mode, M_{cr} is the moment at the support

On average, the calculation error is 12% on the safe side (positive values). The maximum error of the proposed method does not exceed 25%, remaining strictly conservative. Overestimation of the buckling capacity across all cases is limited to less than 10%. The analytically calculated M_{cr} values are obtained assuming no restraints at the ends of the unbraced lengths (μ=1). These results can be refined by taking into account warping and lateral restraints using the effective length factor μ<1.

6. DISCUSSION

The critical buckling moment value M_{cr} is determined when calculating according to the developed method (formula (19)).

For profiles where the load acts along the major principal axis of inertia (i.e. $\alpha_0 = 0$, $k_\alpha = 1$ and $\beta_{res} = \beta_y$), the equation for the critical moment is expressed as follows:

$$M_{cr} = \frac{\pi^2 EI_y}{(\mu l)^2} \cdot C_1 \cdot \left(\left(C_{III} \cdot \beta_y + \frac{e_{y,c}}{2\pi^2} \cdot C_{II} \right) + \sqrt{\left(C_{III} \cdot \beta_y + \frac{e_{y,c}}{2\pi^2} \cdot C_{II} \right)^2 + \frac{I_\omega}{I_y} + \frac{GI_t}{\pi^2 EI_y} \cdot (\mu l)^2} \right) \quad (20)$$

The actual LTB capacity of a beam, considering the structural configuration of its support joints, typically exceeds the analytical solution obtained from an idealized model with free warping boundaries [18, 21] as also demonstrated by the results of the present study (Tables 5–7). To account for the end restraints the effective-length factor μ is provided in the proposed methodology. Future studies aim to evaluate and recommend effective length factors for various boundary conditions to enhance the accuracy of the methodology.

According to the Russian steel design code SP 16.13330.2017, the lateral-torsional buckling analysis of flexural members is performed using the formula: $\frac{M_x}{\varphi_b W_{x,c} R_y \gamma_c} \le 1$,

where $W_{x,c}$ is the section modulus of the compression flange; $\varphi_b = \frac{\sigma_{cr}}{R_y}$ is the LTB reduction factor which relates the critical buckling stress σ_{cr} to the design yield strength of the steel R_y.

To adapt the proposed method to the verification format of SP 16.13330.2017, the critical stresses can be expressed: $\sigma_{cr} = \frac{M_{cr}}{W_{x,c}}$,

where M_{cr} is the critical buckling moment (for the mid-span mode M_{cr} is the maximum moment in the span; for the support-zone mode it is the moment at the support).

7. CONCLUSIONS

Based on theoretical and numerical investigations, and taking into account available experimental data, a practical method for the lateral-torsional buckling analysis of thin-walled beams with open asymmetric cross-sections has been developed. The method is applicable to both simply supported and continuous beams. The key outcomes, assumptions, and future prospects of this research are summarized below:

1. Elastic lateral-torsional buckling is considered.
2. Uniaxial bending within the major principal plane of inertia is considered as the primary case. An analytical solution for biaxial bending is also provided, which is relevant for sections where web-plane loads induce unsymmetrical bending (for example Z-profile).
3. Transverse loads passing through the shear center are considered to eliminate pre-buckling torsion. For eccentric loading, the induced torque makes the serviceability limit state criteria decisive. Due to the low torsional stiffness of open thin-walled sections, the twist angle exceeds the limiting value well before reaching the critical buckling load [17, 18].
4. Channels and similar cross-sections with the shear center located outside the profile are analyzed assuming the load acts centrally. This approach accounts for the structural conditions of

load transfer across the entire flange width. However, a serviceability limit state criteria check must be conducted in addition to the buckling stability assessment

5. The scientific novelty of the research lies in:

- the analytical determination of the C_I, C_{II} and C_{III} coefficients derived directly from the differential buckling equations;
- the derivation of formulas for analyzing thin-walled beams under unsymmetrical bending.

6. The primary advantages of the proposed methodology are as follows:

- versatility across various cross-sectional shapes, arbitrary loading scenarios, and boundary conditions;
- comprehensive consideration of actual bending moment diagrams, load application heights, load directions, and cross-sectional asymmetry;
- compliance with the standard verification formats of SP 16.13330 ensuring seamless integration into national design codes.

7. Future research will focus on the following:

- investigation of end restraint stiffness under actual structural configurations of beam support joints and intermediate braces;
- refinement of the effective-length factor values to account for warping, bending, and lateral restraints at the ends of the unbraced length;
- analysis of the effects of plastic deformations, initial imperfections [22], and residual stresses;
- development of design recommendations for the buckling stability assessment of steel columns and rafters within tapered frames [23];
- implementation of the methodology into a software package, including its application within digital standards and design codes.

REFERENCES

1. **Timoshenko S.P.** (1955) *Ustojchivost' uprugikh sistem* [Stability of elastic systems]. Moscow: Gostekhizdat. (in Russian)
2. **Bleich F.** (1952) *Buckling strength of metal structures*, New York: McGraw-Hill.
3. **White D.V., Jung S.-K**. (2003) *Simplified Lateral Torsional Buckling Equations for Singly-Symmetric I-Section Members*, Structural Engineering, Mechanics and Materials Report No. 03-24b, School of Civil and Environmental Engineering, Georgia Insitutute of Technology, Atlanta, GA
4. **Ziemian R. D.** (2010) *Guide to stability design criteria for metal structures (6th ed.)*. John Wiley & Sons, Inc.
5. **Clark J.W., Hill H.N.** (1960) Lateral Buckling of Beams. *Journal of the Structural Division*, vol. 86, pp. 175-196. doi: 10.1061/JSDEAG.0000540
6. **Andrade A., Camotim D., Costa P.P.** (2007) On the evaluation of elastic critical moments in doubly and singly symmetric I-section cantilevers. *Journal of Constructional Steel Research*, vol. 63 (7), pp. 894–908. doi: 10.1016/j.jcsr.2006.08.015
7. **Bureau A.**, NCCI: Elastic critical moment for lateral torsional buckling. In SN003a-EN-EU NCCI
8. **Boissonade N., Greiner R., Jaspart J. P.** Rules for Member Stability in EN 1993-1-1: Background documentation and design guidelines. (ECCS, Brussels, 2006)
9. **Mathew D.B., Girija K., Nazeer M., Anagha N., Vengadesh J. K. V.** (2024) Experimental and numerical analysis of lateral–torsional bucklingbehaviour of monosymmetric simply supported beam. *Asian Journal of Civil Engineering*, vol. 25, pp. 2471-2482. doi: 10.1007/s42107-023-00920-x.
10. **Mohri F., Brouki A., Roth J.C.** (2003) Theoretical and numerical stability analyses of unrestrained, mono-symmetric thin-walled beams. *Journal of Constructional Steel Research,* vol. 59 (1), pp. 63-90. doi: 10.1016/S0143-974X(02)00007-X.
11. **Mathew D. B., Vengadesh J. K. V., Nazeer M.** (2022) Influence of moment modification factor in lateral torsional buckling of doubly and monosymmetric sections. Proceedings of the *12th Structural Engineering Convention—An International Event (SEC 2022), ASPS Conference Proceedings (Jaipur, India, December 19-22,*

2022), vol. 1, pp. 427–433. doi:10.38208/acp.v1.530.
12. **Bijak R.** (2019) Lateral-torsional buckling moment of simply supported unrestrained monosymmetric beams. *IOP Conference Series: Materials Science and Engineering*, vol. 471 (3), 032074. doi:10.1088/1757-899X/471/3/032074.
13. **Hauksson H., Vilhjalmsson J.B.** (2014) *Lateral-torsional Buckling of Steel Beams with Open Cross Section: Elastic Critical Moment Study and Software Application* (Master's Thesis), Gothenburg: Chalmers University of Technology.
14. **Farfel M.I., Gukova M.I., Svyatoshenko A.E.** (2022) Obshchaya ustoychivost' balok dvutavrovogo postoyannogo secheniya. Razvitie raschetnykh polozheniy [Total stability of two constant section beams. Development of payment provisions]. *Structural Mechanics and Analysis of Constructions,* no. 1, pp. 4–13. doi: 10.37538/0039-2383.2022.1.4.13
15. **Ilyushenkov A.O.** (2025) Razvitie inzhenernoy metodiki rascheta ustoychivosti ploskoy formy izgiba dvutavrovoy balki [Development of engineering methodology for calculating the plane bending stability of an I-beam]. *Bulletin of Science and Research Center of Construction*, vol. 46 (3), pp. 22-42. doi: 10.37538/2224-9494-2025-3(46)-22-42.
16. **Белый Г.И.** Деформационный расчет и устойчивость стержневых элементов стальных конструкций с несимметричным сечением // Вестник гражданских инженеров. 2021. № 4 (87). С. 44-54. doi: 10.23968/1999-5571-2021-18-4-44-53
17. **Туснин А.Р.** Расчет и проектирование конструкций из тонкостенных стержней открытого профиля: дис. … докт. техн. наук. М., 2003. 427 с
18. **Туснина О.А.** Анализ общей устойчивости швеллера при изгибе (2025) Сборник докладов V Национальной научной конференции (г. Москва, 16 декабря 2024 г.)
19. **Vlasov V.Z.** (1959) *Tonkostennye uprugie sterzhni* [Thin–walled elastic members]. Moscow: Fizmatgiz. (in Russian)
20. **Kitipornchai S., Wang C.M., Trahair N.S.** (1986) Buckling of monosymmetric I-beams under moment gradient. *Journal of the Structural Division*, vol. 112 (ST4), pp 781-799. doi: 10.1061/(ASCE)0733-9445(1986)112:4(781)
21. **Lebastard M., Couchaux M., Santana M.V.B., Bureau A., Hjiaj M.** (2022) Elastic lateral-torsional buckling of beams with warping restraints at supports. *Journal of Constructional Steel Research*, vol. 197, 107410. doi: 10.1016/j.jcsr.2022.107410.
22. **Abu Reden G.A., Adany S.** (2025) Elastic lateral-torsional buckling of single-span doubly symmetric I-section beams with intermediate discrete lateral support considering prebuckling deflections. *Thin-Walled Structures*, vol. 212, 113179. doi: 10.1016/j.tws.2025.113179.
23. **Katyushin V.V.** (2018) Zdaniya s karkasami iz stal'nykh ram peremennogo secheniya [Buildings with frames made of tapered steel members]. Moscow: ASV (in Russian).

СПИСОК ЛИТЕРАТУРЫ

1. **Тимошенко С.П.** Устойчивость упругих систем. – М.: Гостехиздат, 1955. – 567 с.
2. **Блейх Ф.** Устойчивость металлических конструкций. – М.: Физматгиз, 1959. – 544 с.
3. **White D.V., Jung S.-K.** Simplified Lateral Torsional Buckling Equations for Singly-Symmetric I-Section Members, Structural Engineering, Mechanics and Materials Report No. 03-24b, School of Civil and Environmental Engineering, Georgia Insitutute of Technology, Atlanta, GA, 2003
4. **Ziemian R.D.** Guide to stability design criteria for metal structures (6th ed.). John Wiley & Sons, Inc., 2010

5. **Clark J.W., Hill H.N.** Lateral Buckling of Beams // Journal of the Structural Division, 1960, Vol. 86, pp. 175-196. doi: 10.1061/JSDEAG.0000540
6. **Andrade A., Camotim D., Costa P.P.** (2007) On the evaluation of elastic critical moments in doubly and singly symmetric I-section cantilevers // Journal of Constructional Steel Research, 2007, Vol. 63 (7), pp. 894–908. doi: 10.1016/j.jcsr.2006.08.015
7. **Bureau A.**, NCCI: Elastic critical moment for lateral torsional buckling. In SN003a-EN-EU NCCI
8. **Boissonade N., Greiner R., Jaspart J. P.** Rules for Member Stability in EN 1993-1-1: Background documentation and design guidelines. (ECCS, Brussels, 2006)
9. **Mathew D.B., Girija K., Nazeer M., Anagha N., Vengadesh J. K. V.** Experimental and numerical analysis of lateral–torsional bucklingbehaviour of monosymmetric simply supported beam // Asian Journal of Civil Engineering, 2024, Vol. 25, pp. 2471-2482. doi: 10.1007/s42107-023-00920-x.
10. **Mohri F., Brouki A., Roth J.C.** Theoretical and numerical stability analyses of unrestrained, mono-symmetric thin-walled beams // Journal of Constructional Steel Research, 2003, Vol. 59 (1), pp. 63-90. doi: 10.1016/S0143-974X(02)00007-X.
11. **Mathew D. B., Vengadesh J. K. V., Nazeer M.** (2022) Influence of moment modification factor in lateral torsional buckling of doubly and monosymmetric sections // Proceedings of the 12th Structural Engineering Convention—An International Event (SEC 2022), ASPS Conference Proceedings (Jaipur, India, December 19-22, 2022), vol. 1, pp. 427–433. doi:10.38208/acp.v1.530.
12. **Bijak R.** Lateral-torsional buckling moment of simply supported unrestrained monosymmetric beams // IOP Conference Series: Materials Science and Engineering, 2019, Vol. 471 (3), 032074. doi:10.1088/1757-899X/471/3/032074.
13. **Hauksson H., Vilhjalmsson J.B.** Lateral-torsional Buckling of Steel Beams with Open Cross Section: Elastic Critical Moment Study and Software Application (Master's Thesis), 2014, Gothenburg: Chalmers University of Technology
14. **Фарфель М.И., Гукова М.И., Святошенко А.Е.** Общая устойчивость балок двутаврового постоянного сечения. Развитие расчетных положений // Строительная механика и расчет сооружений, 2022, № 1. С. 4–13. doi: 10.37538/0039-2383.2022.1.4.13
15. **Ильюшенков А.О.** Развитие инженерной методики расчета устойчивости плоской формы изгиба двутавровой балки // Вестник НИЦ «Строительство», 2025, Том 46, № 3. С. 22-42. doi: 10.37538/2224-9494-2025-3(46)-22-42.
16. **Белый Г.И.** Деформационный расчет и устойчивость стержневых элементов стальных конструкций с несимметричным сечением // Вестник гражданских инженеров, 2021, № 4 (87). С. 44-54. doi: 10.23968/1999-5571-2021-18-4-44-53
17. **Туснин А.Р.** Расчет и проектирование конструкций из тонкостенных стержней открытого профиля: дис. … докт. техн. наук. М., 2003. 427 с
18. **Туснина О.А.** Анализ общей устойчивости швеллера при изгибе // Актуальные проблемы строительной отрасли и образования: сборник докладов V Национальной научной конференции (г. Москва, 16 декабря 2024 г.). М.: Издательство МИСИ – МГСУ, 2025. С. 84-89.
19. **Власов В.З.** Тонкостенные упругие стержни. – М.: Физматгиз, 1959 – 568 с.
20. **Kitipornchai S., Wang C.M., Trahair N.S.** Buckling of monosymmetric I-beams under moment gradient // Journal of the Structural Division, 1986, Vol. 112 (ST4), pp 781-799. doi: 10.1061/(ASCE)0733-9445(1986)112:4(781)
21. **Lebastard M., Couchaux M., Santana M.V.B., Bureau A., Hjiaj M.** (2022) Elastic lateral-torsional buckling of beams with

warping restraints at supports // Journal of Constructional Steel Research, 2022, Vol. 197, 107410. doi: 10.1016/j.jcsr.2022.107410.

22. **Abu Reden G.A., Adany S.** (2025) Elastic lateral-torsional buckling of single-span doubly symmetric I-section beams with intermediate discrete lateral support considering prebuckling deflections // Thin-Walled Structures, 2025, Vol. 212, 113179. doi: 10.1016/j.tws.2025.113179.
23. **Катюшин В.В.** Здания с каркасами из стальных рам переменного сечения. – М.: Издательствово АСВ, 2018. – 1077 с.

Olga A. Tusnina, candidate of technical sciences, docent, associated professor, Department of Steel and Wooden Structures, National Research Moscow State University of Civil Engineering (NRU MGSU), 26, Yaroslavskoe Shosse, Moscow, 129337, Russia, e-mail: tusninaOA@mgsu.ru

Ольга Александровна Туснина, кандидат технических наук, доцент, доцент кафедры Металлических и деревянных конструкций, Национальный исследовательский Московский государственный строительный университет (НИУ МГСУ), д. 26, Ярославское шоссе, г. Москва, 129337, Россия, e-mail: tusninaOA@mgsu.ru